FULL PAPER

Magnetic Resonance in Medicine 00:00–00 (2014)

Four-Dimensional Flow Assessment of Pulmonary Artery Flow and Wall Shear Stress in Adult Pulmonary Arterial Hypertension: Results from Two Institutions

Alex J. Barker,[1]* Alejandro Roldán-Alzate,[2] Pegah Entezari,[1] Sanjiv J. Shah,[3] Naomi C. Chesler,[4] Oliver Wieben,[2] Michael Markl,[1,5] and Christopher J. François[2]

Purpose: To compare pulmonary artery flow using Cartesian and radially sampled four-dimensional flow-sensitive (4D flow) MRI at two institutions.

Methods: Nineteen healthy subjects and 17 pulmonary arterial hypertension (PAH) subjects underwent a Cartesian 4D flow acquisition (institution 1) or a three-dimensional radial acquisition (institution 2). The diameter, peak systolic velocity (Vmax), peak flow (Qmax), stroke volume (SV), and wall shear stress (WSS) were computed in two-dimensional analysis planes at the main, right, and left pulmonary artery. Interobserver variability, interinstitutional differences, flow continuity, and the hemodynamic measurements in healthy and PAH subjects were assessed.

Results: Vmax, Qmax, SV, and WSS at all locations were significantly lower ($P < 0.05$) in PAH compared with healthy subjects. The limits of agreement were 0.16 m/s, 2.4 L/min, 10 mL, and 0.31 N/m^2 for Vmax, Qmax, SV, and WSS, respectively. Differences between Qmax and SV using Cartesian and radial sequences were not significant. Plane placement and acquisition exhibited isolated, site-based differences between Vmax and WSS.

Conclusions: 4D flow MRI was used to detect differences in pulmonary artery hemodynamics for PAH subjects. Flow and WSS in healthy and PAH subject cohorts were similar between Cartesian- and radial-based 4D flow MRI acquisitions with minimal interobserver variability. **Magn Reson Med 000:000–000, 2014. © 2014 Wiley Periodicals, Inc.**

Key words: pulmonary hypertension; 4D flow MRI; wall shear stress

INTRODUCTION

Pulmonary hypertension (PH) is associated with substantial morbidity and mortality. The disease is characterized by an increase in pulmonary artery pressure and stiffening of the proximal pulmonary arteries (PAs). The result is an increase in right ventricular (RV) afterload and ultimately RV failure (1–3). Based on the underlying etiology, pathology and therapeutic response, the World Health Organization (WHO) categorizes PH into five categories (4). Yet for all PH categories, survival rates are poor, and research efforts are complicated by the multifactorial nature of the disease.

For patients with PH, particularly those with pulmonary arterial hypertension (PAH), cardiovascular magnetic resonance (CMR) is used increasingly to assess cardiac function in order to detect early changes in RV function caused by elevated arterial pressure. Given the accuracy compared with alternative modalities, CMR, using CINE balanced steady-state free precession sequences (bSSFP), is considered the gold standard for quantification of both left (5–7) and right (8–10) ventricular size and function. CMR also allows for time-resolved three-dimensional (3D) phase-contrast MRI with three-directional velocity encoding (four-dimensional flow-sensitive [4D flow] MRI), which offers the opportunity to noninvasively measure 3D hemodynamic changes in the pulmonary arteries (11–13). The combination of these techniques provides the opportunity to obtain greater insight regarding the impact PAH has on interactions between the pulmonary vasculature and right ventricle (i.e., ventriculo-vascular coupling). The ability to investigate these interactions in PH subjects is especially relevant given the observation of drastic changes in the PA hemodynamic environment (11–13).

Functional characterization of the RV and advanced CMR flow measurements are increasingly important given that PAH is not merely a disease of the distal vessels, as the proximal pulmonary arteries also undergo dilation, remodeling, and stiffening (14–16). These distal and proximal pulmonary arterial changes not only contribute to decreased compliance and increased resistance (15,16), thereby increasing RV afterload (17), they also alter secondary flows (such as helix and vortex formation), including changes to the velocity profile shape and magnitude (13,18,19). These complex flow changes are only beginning to be understood in the context of their impact on wall shear stress (WSS), control of smooth muscle cell tone via mechano-transduction, and vascular remodeling that alters intrinsic proximal tissue characteristics

[1]Department of Radiology, Northwestern University Feinberg School of Medicine, Chicago, Illinois, USA.

[2]Departments of Radiology & Medical Physics, University of Wisconsin, Madison, Wisconsin, USA.

[3]Division of Cardiology, Northwestern University Feinberg School of Medicine, Chicago, Illinois, USA.

[4]Department of Biomedical Engineering, University of Wisconsin, Madison, Wisconsin, USA.

[5]Department of Biomedical Engineering, Northwestern University, Chicago, Illinois, USA.

Grant sponsor: National Institutes of Health; Grant numbers: R01HL072260, R01HL105598, R01HL086939, R01HL115828, UL1RR025741; Grant sponsor: National Center for Advancing Translational Sciences Clinical and Translational Science Award program; Grant number: 9U54TR000021; (previously grant number 1UL1RR025011 through the National Center for Research Resources); Grant sponsor: American Heart Association; Grant numbers: Scientist Development; 13SDG14360004. The Departments of Radiology and Medical Physics at the University of Wisconsin-Madison receive support from GE Healthcare.

*Correspondence to: Alex Barker, Ph.D., Department of Radiology, Northwestern University, Feinberg School of Medicine, 737 N. Michigan Ave., Suite 1600, Chicago, IL. E-mail: alex.barker@northwestern.edu

Received 24 February 2014; revised 27 May 2014; accepted 27 May 2014

DOI 10.1002/mrm.25326

Published online 00 Month 2014 in Wiley Online Library (wileyonlinelibrary.com).

Table 1
Summary of Subject Demographics

	Institution 1		Institution 2		Combined	
	Controls	PAH	Controls	PAH	Controls	PAH
Sex, M:F	8:1	5:5	6:4	1:6	14:5	6:11
Age, y	40 ± 12	58 ± 10*	37 ± 14	55 ± 9*	39 ± 13	57 ± 10*
Heart rate (bpm)	69 ± 6	73 ± 5	57 ± 7†	74 ± 9*	63 ± 9	74 ± 7**
WHO, group (n)	—	1(8), 4(2)	—	1(6), 3(1)	—	1(14), 3(1), 4(2)
NYHA, class (n)	—	2(6), 3(4)	—	2(2), 3(5)	—	2(8), 3(9)
Mean PAP, mmHg	—	47 ± 18	—	39 ± 14	—	45 ± 17
Pulmonary vascular resistance (PVR)	—	436 ± 208	—	514 ± 251	—	490 ± 236
Years of PAH	—	2.4 ± 2.1	—	0.8 ± 0.9†	—	1.5 ± 1.9

Values are presented as the mean ± standard deviation unless noted otherwise. PAH groups are based on WHO classification.
*$P < 0.05$ by Wilcoxon rank-sum test vs. control groups.
**$P < 0.001$ by Wilcoxon rank-sum test vs. control groups.
†$P < 0.05$ by Wilcoxon rank-sum test as compared between sites.

(19–21). However, given the relative rarity of PAH, large-scale population-based studies will have to involve multiple centers. In order for this to be feasible, cross-platform MR studies must provide similar and consistent results. Additionally, 4D flow MRI is gaining significant interest from the research community (22); however, it has only been used in small, single-center studies.

Therefore, the primary aim of this two-center study was to determine whether PA flow and WSS differences can be detected using two different 4D flow MRI acquisition strategies, using PAH patients and healthy subjects. The secondary aim was to contribute to ongoing efforts regarding the characterization of PA hemodynamics in healthy and PAH subjects.

METHODS

Subjects

The inclusion criteria for patients were as follows: a diagnosis or initial evaluation for idiopathic PAH, systemic sclerosis PAH, or chronic thromboembolic PH; referral for a clinically necessary right heart catheterization; and age between 18 and 80 years. Exclusion criteria were one or more of the following: recent syncope, contraindication to cardiac MRI, mixed etiology PAH (e.g., idiopathic PAH and a history of isolated pulmonary emboli), severe lung disease, and pregnancy. Thus, PAH patients were consecutively recruited if they: 1) met the inclusion/exclusion criteria for the study; 2) consented to the study; and 3) were undergoing clinically indicated right heart catheterization. Informed consent was obtained for all studies, which were conducted according to local institutional review board approved protocols and were compliant with the Health Insurance Portability and Accountability Act. Nine healthy subjects and 10 subjects with PAH were recruited at institution 1 and 10 healthy subjects and seven subjects with PAH were recruited at institution 2. The demographic data on all enrolled subjects are summarized in Table 1.

MRI Studies

Institution 1

MRI studies were performed at 1.5T and 3.0T (Espree, Avanto, Skyra, Siemens Erlangen, Germany). For the assessment of pulmonary blood flow, the 4D flow technique was implemented using a standard Cartesian k-space trajectory in a sagittal oblique 3D volume covering the central pulmonary arteries after venous administration of either gadofosveset trisodium (Ablavar, Lantheus Medical Imaging, North Billerica, Massachusetts, USA) or gadobenate dimeglumine (Multihance, Bracco Diagnostics Inc, Monroe Township, New Jersey, USA). Prospective electrocardiographic gating was used during free breathing with a respiratory navigator located at the lung–liver interface. The pulse sequence parameters were as follows: echo time =2.4–2.7; pulse repetition time = 4.8–5.1 ms; flip angle $\alpha = 10°–15°$; temporal resolution = 38.4–40.8 ms; field of view = 350–440 × 175–220 mm; spatial resolution = 2.2–2.75 × 2.2–2.75 × 2.4–3.2 mm. Velocity sensitivity was adjusted to minimize velocity aliasing (venc = 1.5 m/s) (23).

Institution 2

MRI studies were performed on a 3.0T clinical system (MR750, GE Healthcare, Waukesha, Wisconsin, USA). 4D flow MRI was acquired using a radially undersampled, time-resolved, 3D, three-directional, velocity-encoded imaging sequence (phase contrast with vastly undersampled isotropic projection reconstruction [PC-VIPR]) (24) after venous administration of gadobenate dimeglumine (Multihance, Bracco Diagnostics Inc). A 3D volume covering the chest (centered over the heart) was used. Retrospective reconstruction using electrocardiographic gating and respiratory triggering using bellows with an adaptive acceptance window of 50% was performed. The PC-VIPR sequence parameters were as follows: echo time = 2.1–3.2 ms; pulse repetition time = 6.1–8.9 ms; flip angle $\alpha = 10°–14°$; field of view = 320 × 320 × 220 mm; readout length = 256 samples; spatial resolution = 1.3 mm isotropic. Velocity sensitivity was adjusted to minimize velocity aliasing (venc = 0.75–1.5 m/s) Data were retrospectively sorted into 20 time frames according to their position in the cardiac cycle using a temporal filter similar to Cartesian view sharing (25). This translates into a 41–52 ms temporal resolution, depending on the heart rate (the range is the average between the normal and patient population).

MRI Analysis

Analysis of the 4D flow MRI data (aggregated from both sites) was conducted by two investigators, one at each site. Quantitative flow analysis of the 4D flow MRI datasets was performed using a previously described MATLAB program (MathWorks, Natick, Massachusetts, USA) (26). Briefly, at both institutions, all 4D flow MRI data were preprocessed to correct for eddy currents using a planar fit to static tissue (27). Next, a phase contrast magnetic resonance angiogram was generated, which allowed the user to interactively place two-dimensional cutplanes (CEI Ensight, Apex, North Carolina, USA) perpendicular to the direction of the flow in the main pulmonary artery (MPA), right pulmonary artery (RPA), and left pulmonary artery (LPA). Figure 1 indicates the locations of the MPA, RPA, or LPA cutplanes, which were placed approximately 1 cm downstream from the pulmonary valve or LPA/RPA bifurcation, respectively. Manual segmentation of the vessel wall was performed on the two-dimensional (2D), time-resolved cutplanes and diameter (D), peak systolic velocity (Vmax), peak flow (Qmax), stroke volume (SV), and WSS in the MPA, RPA, and LPA were computed. In addition, cardiac output (CO) was computed by multiplying the heart rate with the SV. The internal consistency of the total flow measurements was assessed by a linear regression of SV through the MPA to the sum of SV through the RPA and LPA. Conservation of mass was considered "upheld" if the slope of the regression approached unity (within 10% error). In order to understand the contribution of complex flow (such as helical flow) to the WSS magnitude, the contribution of in-plane WSS (i.e., "in the plane" of the lumen circumference, as opposed to "through-plane") was reported as a percentage of overall WSS magnitude.

Statistical Analysis

Continuous values are reported as the mean $\pm$ standard deviation. Kruskal-Wallis rank-sum and Fisher's exact tests were used to assess group differences in continuous and categorical variables, respectively. A Wilcoxon rank-sum test was applied to test for intergroup differences, if deemed appropriate by the Kruskal-Wallis rank-sum test. Multiple linear regressions were used to assess differences in flow parameters due to pulmonary hypertension and site/sequence differences; separate analyses were performed for each possible combination of flow parameter, reader, and pulmonary artery branch. These models are identical to two-way (additive) analysis of variance. Bland-Altman 95% limits of agreement were obtained to assess the typical discrepancy between readers. Linear regression of the differences on the means was fitted to assess whether the difference (bias) varied systematically as a function of the average reading. Separate estimates were obtained for each flow parameter and pulmonary artery branch. $P < 0.05$ (two-sided) was the criterion for statistical significance. All statistical computations were performed in R (R Development Core Team, Vienna, Austria).

RESULTS

Subject Demographics

Age, WHO category (group) of PH, New York Heart Association (NYHA) functional class, mean pulmonary artery pressure (mPAP), pulmonary vascular resistance, and years since diagnosis are presented in Table 1. Age, mPAP, and pulmonary vascular resistance were not significantly different between the two sites for patients or controls. A significant difference did exist between the age of the controls and the age of the patients at both sites. Heart rate and years since diagnosis of PAH were significantly different between the two sites, with institution 1 having an average of 0.8 ± 0.9 years and institution 2 an average of 2.4 ± 2.1 years since time of diagnosis to time of MR study. WHO group I (PAH) was the most common form of PH at both institutions, and all PAH patients had either NYHA functional class 2 or 3 symptoms (the mode being NYHA class 2 at institution 1 [n = 6] and class 3 at institution 2 [n = 5]).

Control vs. PAH: PA Size, Bulk Flow, and WSS

For both institutions, 4D flow imaging was successfully performed in all patients. D, Vmax, Qmax, SV, CO, and WSS are summarized for healthy subjects and PAH subjects in Table 2. Significant differences between D, Vmax, Qmax, SV, and WSS existed between control and PAH subjects at both institutions individually and combined (see Table 2 for details). A significant difference existed between normal and PAH subjects for cardiac output at institution 1. The general trend was for the diameter to be enlarged and for the Vmax, Qmax, SV, and WSS parameters to be lower in the PAH population (9 of 12 comparisons at institution 1 and 8 of 12 comparisons at institution 2). For the Cartesian and PC-VIPR sequence, regressions between MPA SV and the sum of SV in both the RPA and LPA resulted in a slope of 0.91 and 0.92 and a Pearson correlation coefficient of 0.89 and 0.95, respectively (Fig. 2). The regional MPA, RPA, and LPA WSS values were significantly lower in PAH subjects than in healthy controls, irrespective of which 4D flow MRI sequence was used (Fig. 3). In addition, the percentage of in-plane WSS was elevated in the MPA and LPA of PAH subjects (Table 2).

Intersite and Interobserver Comparisons

Multiple linear regression analyses were performed for each flow parameter, vascular location, and reader (model structure: flow parameter $\sim$ PAH status + site/sequence). For all subjects with PAH, Qmax, SV, and WSS were significantly lower than controls at all vascular locations, independent of reader and largely by site (Table 3, WSS in the LPA was the only parameter different by site). PAH subjects also had a significantly lower Vmax in the RPA and LPA. Observer 1 found no difference from the controls for MPA Vmax; observer 2 found MPA Vmax lower than the controls. Site differences did exist between Vmax and WSS at the MPA and LPA (Table 3). In summary, 11 of the 12 hemodynamic measurements were independent of reader and 9 of the 12 hemodynamic measurements were independent of site. Interobserver error by Bland-Altman analysis found mean differences for Vmax, Qmax, SV, and WSS in all 36 subjects to be 0.07 m/s, -1.3 L/min, -5 mL, and 0.04 N/m^2, respectively (Fig. 4). The limits of agreement were 0.16 m/s, 2.6 L/min, 10 mL, and 0.31 N/m^2 for Vmax, Qmax, SV, and WSS, respectively.

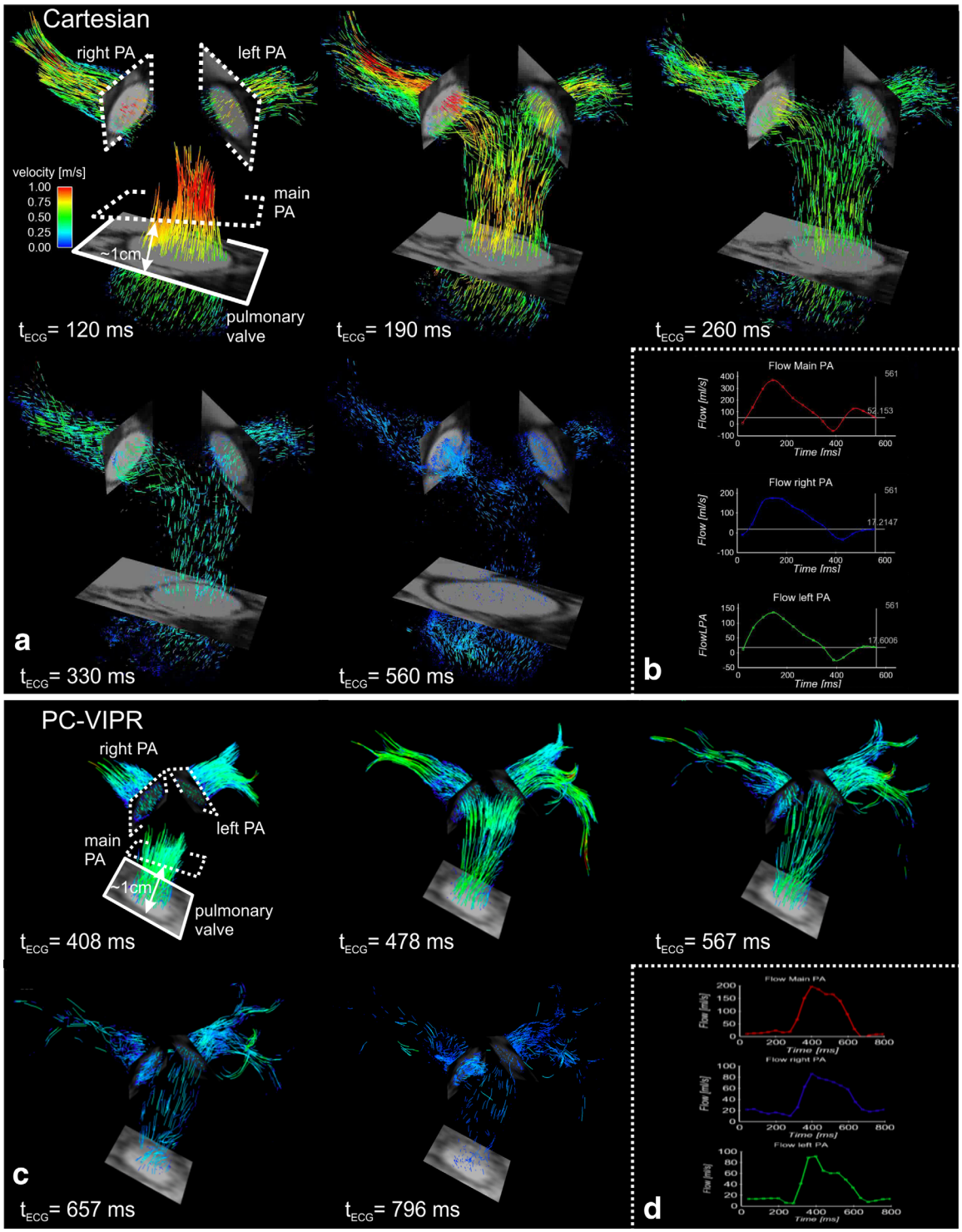

FIG. 1. **(a)** Time-resolved pathline visualization in a volunteer subject from institution 1 (Cartesian acquisition). 2D CINE images at the pulmonary valve and pulmonary branches are included to show vessel morphology. 2D measurement planes (dotted lines) located at the MPA, LPA, and RPA were used for flow quantification (**b**). (**c**) Time-resolved pathline visualization in a volunteer subject from institution 2 (PC-VIPR acquisition). (**d**) Flow quantification for the PC-VIPR examination.

The mean difference had a non-zero slope for stroke volume ($P = 0.002$) and peak flow ($P = 0.011$), thus the 95% confidence intervals are presented in brackets for the bias and limits of agreement (Fig. 4). The agreement of regionally measured WSS, as observed between readers and disease state, is presented in Figure 5.

Disease and Parameter Interactions

Individual univariate regression of Vmax, SV, Qmax, D, and PAH status to WSS revealed that the three most significant correlations to WSS were PAH status (i.e., PAH = "yes" or "no"; $R^2 = 0.52$, $P < 0.001$), D ($R^2 = 0.24$, $P < 0.001$), and Qmax ($R^2 = 0.04$, $P = 0.02$). Figure 6

Table 2
Summary of MPA, RPA, LPA Geometry and Flow Parameters as Measured by Observer 2: Vmax, Qmax, SV, CO, and WSS Magnitude (Averaged Around the Vessel Circumference) as a Function of Disease State

	Institution 1		Institution 2		Combined	
	Controls	PH	Controls	PH	Controls	PH
Diameter, cm						
MPA	1.3 ± 0.1	1.7 ± 0.3*	1.4 ± 0.1	1.7 ± 0.3	1.3 ± 0.1	1.7 ± 0.3**
LPA	0.9 ± 0.1	1.2 ± 0.1**	1.0 ± 0.1	1.2 ± 0.3**	1.0 ± 0.1	1.2 ± 0.2**
RPA	0.8 ± 0.2	1.2 ± 0.2**	1.0 ± 0.1	1.3 ± 0.2**	0.9 ± 0.2	1.3 ± 0.2**
Vmax, m/s						
MPA	0.84 ± 0.13	0.57 ± 0.13*	0.84 ± 0.11	0.82 ± 0.25	0.84 ± 0.12	0.67 ± 0.22**
LPA	0.77 ± 0.18	0.35 ± 0.12**	0.79 ± 0.16	0.62 ± 0.19	0.78 ± 0.16	0.46 ± 0.20**
RPA	0.93 ± 0.17	0.44 ± 0.15**	0.84 ± 0.15	0.65 ± 0.20*	0.88 ± 0.17	0.53 ± 0.20**
Qmax, L/min						
MPA	18.8 ± 4.5	16.2 ± 2.4	21.5 ± 3.9	17.1 ± 6.5	20.2 ± 4.3	16.6 ± 4.4*
LPA	8.1 ± 2.4	5.7 ± 0.9*	10.1 ± 1.7	5.7 ± 1.9*	9.2 ± 2.2	5.7 ± 1.4**
RPA	9.1 ± 2.4	7.7 ± 1.5	11.3 ± 1.9	7.2 ± 3.0*	10.2 ± 2.4	7.5 ± 2.2*
SV, mL						
MPA	68 ± 13	53 ± 12*	88 ± 20	58 ± 26*	79 ± 19	54 ± 20**
LPA	29 ± 8	21 ± 5*	42 ± 10	24 ± 7*	36 ± 11	22 ± 7**
RPA	33 ± 6	26 ± 7	48 ± 11	28 ± 13*	41 ± 12	26 ± 10**
CO, L/min						
MPA	4.7 ± 1.0	3.9 ± 0.8*	4.9 ± 0.6	4.3 ± 1.8	4.8 ± 0.8	4.0 ± 1.3*
LPA	2.0 ± 0.6	1.6 ± 0.4	2.4 ± 0.4	1.8 ± 0.6	2.2 ± 0.5	1.7 ± 0.5*
RPA	2.3 ± 0.4	1.9 ± 0.5	2.7 ± 0.4	2.1 ± 0.9	2.5 ± 0.5	2.0 ± 0.7*
WSS, N/m^2						
MPA (% in-plane)[a]	0.39 ± 0.16 (5)	0.19 ± 0.06* (14)	0.40 ± 0.12 (7)	0.26 ± 0.10* (16)	0.40 ± 0.14 (6)	0.22 ± 0.10** (15)
LPA (% in-plane)[a]	0.34 ± 0.16 (8)	0.12 ± 0.07* (12)	0.48 ± 0.18 (10)	0.21 ± 0.08** (17)	0.41 ± 0.18 (9)	0.16 ± 0.09** (14)
RPA (% in-plane)[a]	0.57 ± 0.24 (14)	0.17 ± 0.05** (13)	0.51 ± 0.16 (16)	0.21 ± 0.07** (18)	0.54 ± 0.21 (15)	0.19 ± 0.07** (15)

Institution 1 was measured using a Cartesian 4D flow MRI acquisition; institution 2 was measured with a radial 4D flow MRI acquisition.
*$P < 0.05$ by Wilcoxon rank-sum compared with each control group, respectively.
**$P < 0.001$ by Wilcoxon rank-sum compared with each control group, respectively.
[a]Values in parentheses indicate percentage of systolic WSS magnitude that is composed of in-plane WSS (as opposed to through-plane).

illustrates the interactions. Multivariate regression of the model "WSS ~ PAH status + D + Qmax" determined PAH status ($P < 0.001$) and D ($P = 0.01$) were significantly correlated to WSS (Qmax was not correlated, $P = 0.68$). The multivariate model exhibited a slightly higher adjusted $R^2 = 0.54$ ($P < 0.001$) when compared with the best univariate correlation.

DISCUSSION

For PAH, right heart catheterization is the gold standard regarding diagnosis, monitoring, and evaluation of therapeutic response. Nonetheless, CMR remains the gold standard for noninvasively measuring RV size and function (5–10). Given recent studies directing attention to the potential disease pathway for flow mediated mechano-transduction and proximal PA remodeling, CMR (specifically 4D flow MRI) can additionally provide advanced functional hemodynamic information. In this respect, 4D flow is especially relevant given that complex 3D flow is known to be present in the enlarged arteries of PAH patients (13,18). However, few multisite studies have investigated whether complex differences in flow between healthy and PAH subjects can be detected, such as those related to WSS. This is especially

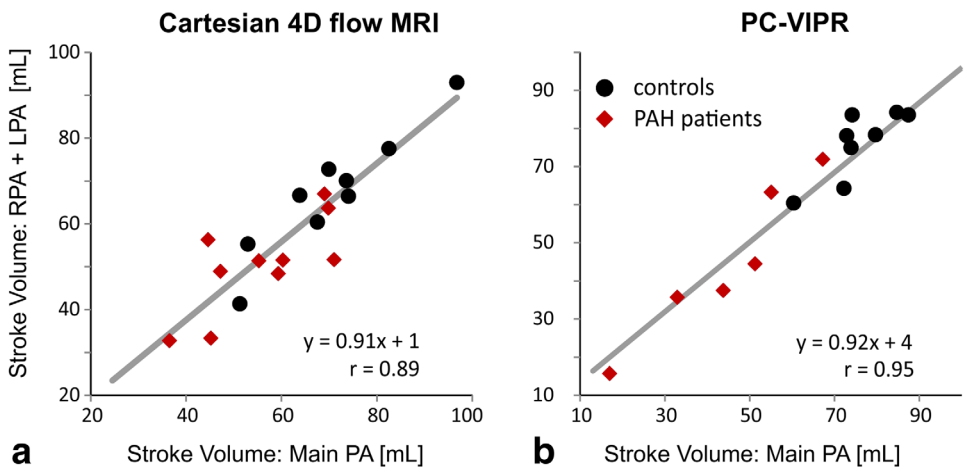

FIG. 2. Conservation of mass (sum of flow through LPA and RPA vs. flow through MPA) for the two 4D flow MRI techniques used to assess pulmonary blood flow. [Color figure can be viewed in the online issue, which is available at wileyonlinelibrary.com.]

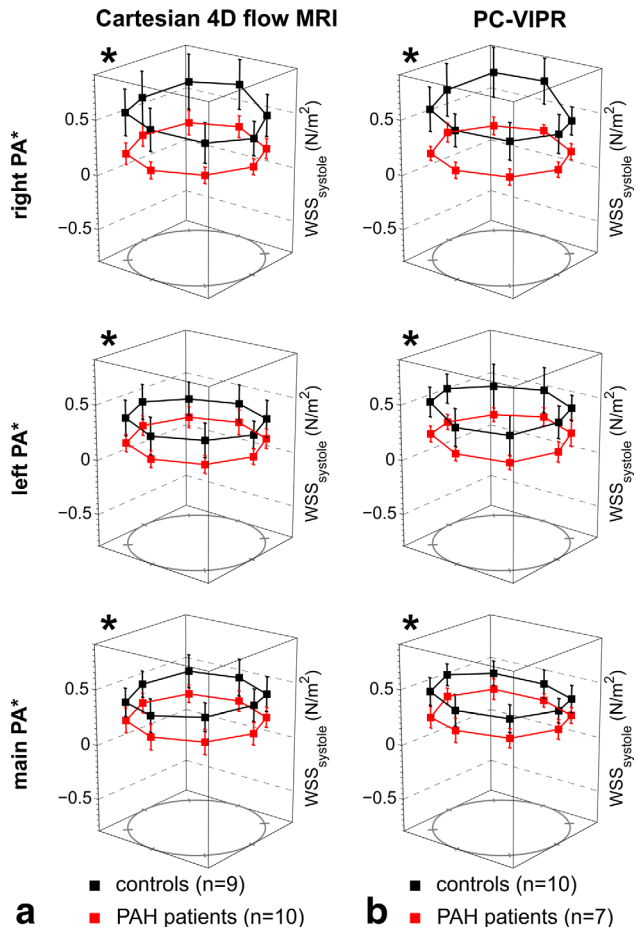

FIG. 3. Comparisons of regional WSS derived from (**a**) Cartesian 4D flow MRI and (**b**) PC VIPR (b) data (observer 2). The individual plots show the WSS distribution in normal controls compared with patients with PAH. Note that both Cartesian 4D flow MRI and PC VIPR were able to detect similar changes in segmental systolic WSS in PAH patients compared with controls. *All measured locations were significantly different between controls and PAH patients for both sequences ($P < 0.01$). [Color figure can be viewed in the online issue, which is available at wileyonlinelibrary.com.]

Table 3
Multiple Linear Regression Results Illustrate Where Significance Differences Occur Between Flow Parameters as a Function of Disease State, Observer, and Site

	MPA	LPA	RPA
Observer 1			
SV	*	**	**
Qmax	*	**	**
Vmax	†	**,†	**
WSS	**	**,‡	**
Observer 2			
SV	**	**	**
Qmax	*	**	*
Vmax	**	**,†	**
WSS	**	**,†	**

*$P < 0.05$ as compared between disease states.
**$P < 0.001$ as compared between disease states.
†$P < 0.05$ as compared between sites.
‡$P < 0.001$ as compared between sites.

true for sites that use fundamentally different 4D flow acquisition strategies. Therefore, in this study, Cartesian and radial 4D flow MRI sequences were used at two separate institutions to quantify pulmonary artery flow and WSS in 19 healthy control subjects and 17 PAH patients. To our knowledge, this is the first multicenter 4D flow MRI study, irrespective of vascular region.

The primary findings of this study support the assertion that changes of flow and WSS in PAH patients can be detected irrespective of CMR acquisition strategy or observer. This is important for future multicenter PAH trials that study the effects of PAH treatment on ventriculo-vascular coupling, because these trials may use CMR systems from different vendors. In particular, site-specific and combined multiple linear regressions indicate that both bulk flow parameters Qmax and SV are significantly depressed in all proximal arteries in the presence of PAH. This is similar to previous reports (11). Additionally, Vmax and WSS were found to be depressed in the LPA and RPA. Qmax and SV in each subject group were similar across both sequences; however, the measurements of Vmax and WSS did exhibit isolated differences depending on site (specifically in the difficult-to-delineate region of the MPA and LPA). Potential reasons may be the spectrum of patient disease between sites (see WHO group, NYHA functional class, and years since diagnosis, Table 1), although sequence differences and noise cannot be ruled out. Nonetheless, as demonstrated by Bland-Altman graphs, the agreement in SV and Qmax between independent, blinded observers was satisfactory. Due to noise, the limits of agreement were higher for Vmax and WSS (Figure 4); however, differences were detectable according to disease state for both observers (Table 3), and good agreement was found for the mean of the regional WSS between observers (Fig. 5). In summary, these results demonstrate that multicenter 4D flow MRI studies can be conducted, even with different 4D flow MRI acquisitions.

Internal consistency was confirmed with the continuity equation and a regression slope resulting in a value within 10% of unity (this acceptance threshold has been used previously for cardiac applications [Fig. 2]) (28). The Pearson correlation of the regression also indicates the robustness of the technique for both sequences. The trend toward lower peak and cardiac output in PAH subjects (Table 2) is concordant with the observations of Ley et al. (11) and Tang et al. (20). Tang et al. reported a total MPA flow of 3.7 ± 1.2 L/min and 5.8 ± 0.6 L/min in PAH and healthy subjects, respectively. Additionally, the increased size of the vessels is in line with previous MR studies (11,29). Slower flow and larger diameter vessels in patients with PAH will result in lower velocity gradients at the proximal PA wall and thus lower WSS. Even in the case of equal flow rate between PAH and healthy subjects, the presence of a dilated artery will generally result in lower velocity gradients at the wall, and thus lower WSS. This result has been demonstrated in pediatric PAH (19) and using computational fluid dynamics (CFD) (20). Additionally, larger vessels are known to promote helical and vortical flow, as has been observed by Reiter et al (13). In this study, we

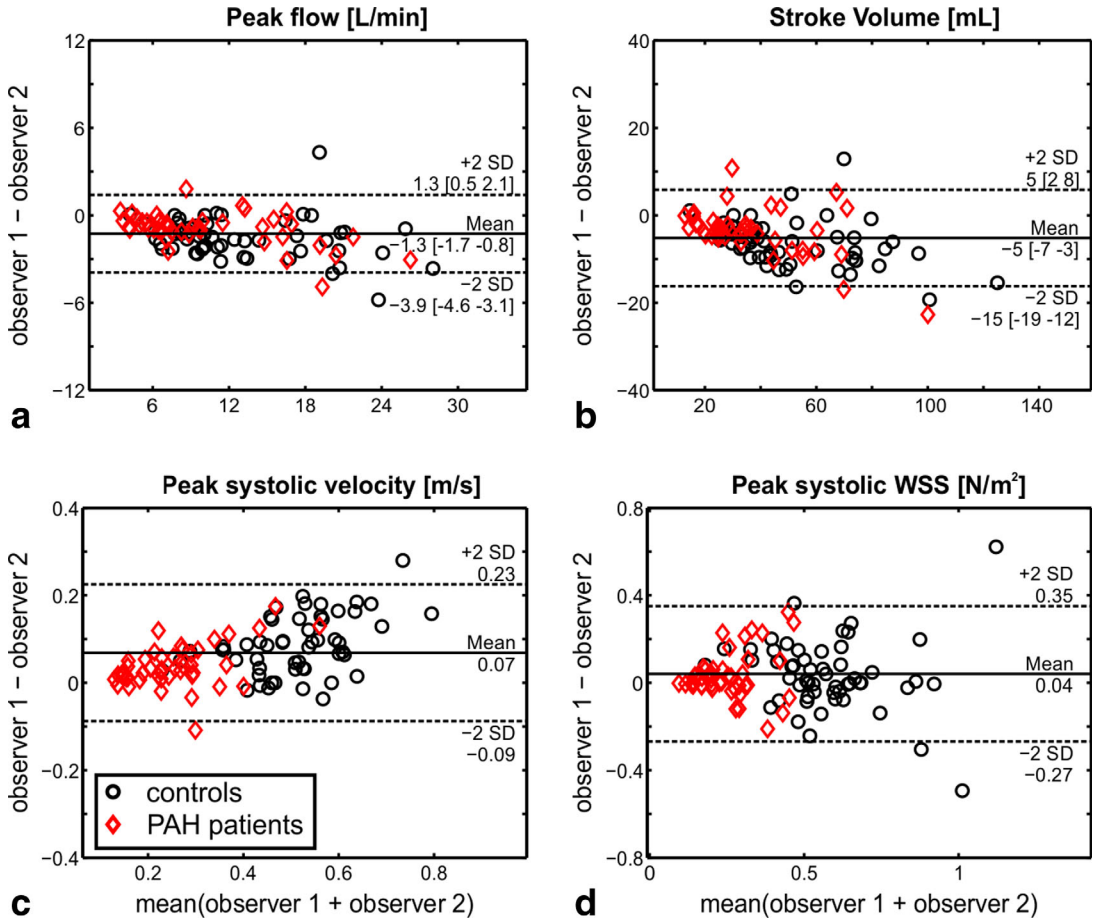

FIG. 4. Bland-Altman analysis of interobserver variability for four different measures of PA hemodynamics (peak flow, total flow, peak velocity, and WSS). Points represent data from 19 healthy controls and 17 PAH patients. For each subject, flow and WSS parameters were evaluated by two independent observers in the three analysis planes (main PA, RPA, and LPA) resulting in n = 3* (19 + 17) = 108 data points for each Bland-Altman plot. If the mean difference exhibited a non-zero slope, 95% confidence intervals are presented in brackets. [Color figure can be viewed in the online issue, which is available at wileyonlinelibrary.com.]

investigated the contribution of the circumferential flow (i.e. in-plane) to the overall WSS magnitude and found that it was increased in the LPA and MPA (Table 2). The elevation of in-plane WSS indicates that helicity and vorticity are increased in these vessels. Interestingly, no elevation of in-plane WSS was found in the RPA. This may be due to the existence of helicity in the RPA of normal patients, as evident in the particle traces of the institution 1 control subject shown in Figure 1, between the trigger time of 190 and 560 ms.

Of note, the mean peak systolic WSS values we calculated using 4D flow MRI are of similar magnitude, but lower than those derived using CFD (2.05 N/m^2 in healthy subjects and 0.43 N/m^2 in PAH subjects). These differences are presumably related to differences in the spatial resolution used to estimate the WSS (26). A previous 2D phase contrast MRI study analyzing RPA WSS in pediatric subjects (at higher spatial resolution, but in smaller, younger subjects), found WSS values on the order of magnitude to those measured in this study, but lower than the CFD study (0.7 N/m^2 in healthy subjects versus 0.2 N/m^2 in PAH subjects) (19). Additional site differences in WSS values found in the PAH subjects may be associated with different stages and severity of disease, thus future studies should take care to recruit homogenous populations to determine the significance of this effect. For example, SV was depressed in the patient population at both sites. However, cardiac output was preserved for institution 2 subjects (although trending lower compared with the control group). This may be indicative of the earlier stage of disease (i.e., years of PAH) and thus the ability to compensate for a drop in SV. In support of this assertion, institution 1 patients had a longer period between diagnoses and MRI study (2.4 ± 2.1 years vs. 0.8 ± 0.9 years).

The long-standing notion that PAH is a disease of the distal vessel is evolving with recent evidence warranting additional investigation regarding the role of proximal pulmonary remodeling in the disease pathway (12,16,17). It is postulated that the proximal PAs stiffen and dilate as a result of collagen accumulation (or elastin loss) and pressure loading, which greatly diminishes the Windkessel effect and the dual-stage RV-PA pump (15,16). This will increase the RV afterload and alter proximal flow dynamics. These changes can be measured in the form of bulk flow (SV, CO, and Qmax) as well as in the form of Vmax and WSS, the latter of which is known to regulate transcription events in vascular remodeling.

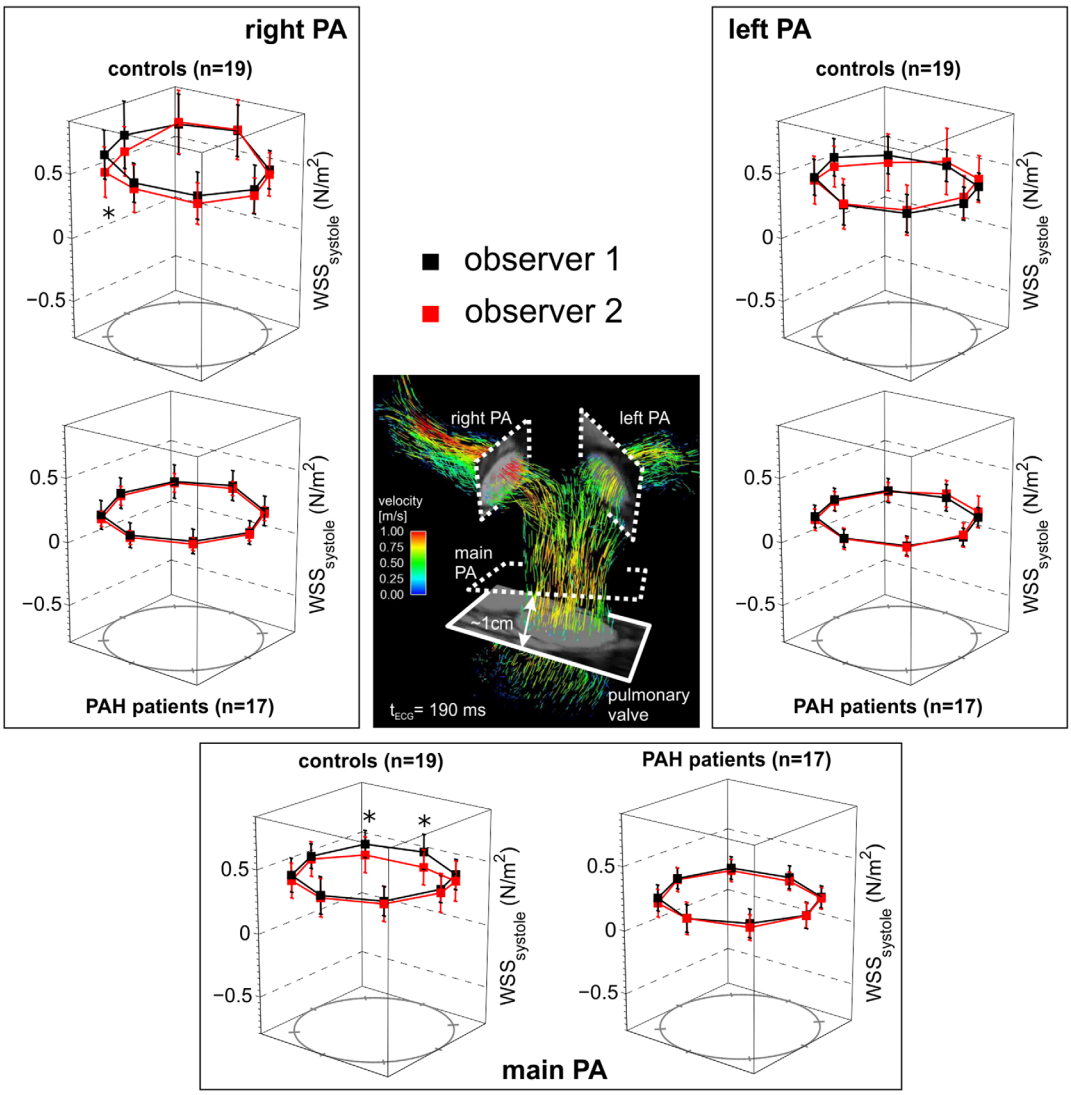

FIG. 5. Interobserver agreement of the segmental analyses of peak systolic WSS in the MPA, LPA, and RPA. Each graph shows the comparison of segmental WSS for all 4D flow data sets (19 healthy controls and 17 PAH patients), which were analyzed by two independent observers blinded to each other's results. [Color figure can be viewed in the online issue, which is available at wileyonlinelibrary.com.]

WSS represents the drag force along the vessel wall caused by a tangential blood velocity and viscosity. It has drawn interest for its role in vascular biology because of a demonstrated role in endothelial function, particularly in systemic circulation (30,31). Specifically, alterations in arterial WSS have been linked to the development of arteriosclerosis and plaque stability (32–34) through its effects on matrix metalloproteinase (33), endothelin-1 (35), and endothelial nitric oxide synthase (36,37) activity. These studies suggest that measuring WSS in patients with PAH may be important to extend our understanding of how changes in the structure of the PAs affect the progression of PAH, and how these characteristics respond to alterations in RV function or therapy. Thus, understanding the changes in both net flow parameters (for coupling effects) and WSS (for mechanotransduction effects) may help elucidate the complex etiology involved in PAH progression. This multisite study is a first effort to understand exactly which parameters

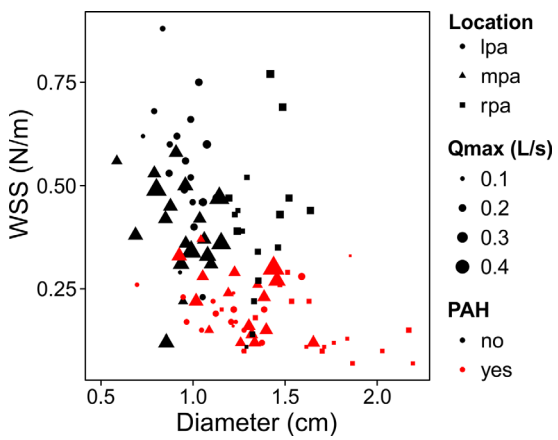

FIG. 6. Systolic WSS (averaged across the circumference of the vessel lumen) as a function of disease state, vessel diameter (D), peak flow rate (Qmax), and measurement location. [Color figure can be viewed in the online issue, which is available at wileyonlinelibrary.com.]

can be measured reliably, in which vascular territory, and how they interact.

In terms of interactions, the univariate models found that WSS correlated largely with a binary description of disease status. However, because age was significantly different between the two populations, age was tested as a confounder by performing individual univariate linear regressions of WSS to age on the PAH-only (age range, 38–74 y) and the volunteer cohorts (age range, 22–60 y). WSS was not related to age for each cohort (PAH-only, $P = 0.32$ and volunteer, $P = 0.11$). Therefore, a multivariate model constructed from the three highest univariate correlations for the entire study population (i.e., PAH status, D, and Qmax), which demonstrated that WSS is most driven by the binary description of disease state ($P < 0.001$), even when the weaker vessel size interactions are taken into account (D, $P < 0.01$). To investigate whether changes in PAH state can be detected beyond a mere "yes/no" model, a multivariate model constructed from the three highest univariate correlations for the PAH-only cohort (i.e., D, mPAP, and Qmax), which found that WSS was driven by Qmax ($P = 0.035$) and more weakly by mPAP ($P = 0.059$). In summary, although size played a moderately significant role for the determination of WSS in both cohorts, the interaction appears to be not as strong as the presence of PAH (both by a binary descriptor, or mPAP) or a decrease in flow in the PAH-only group (Qmax).

Recent CMR studies have shown promise for radiation-free catheterization (38), or noninvasive estimation of mPAP using parametric models (39). These efforts are complemented by 4D flow MRI, which has been used previously to assess the hemodynamics, including derivation of WSS, in the systemic circulation using both Cartesian (26,40,41) and radial acquisitions (42). Using 4D flow MRI in the pulmonary circulation, Reiter et al. (13,18) observed abnormal vortex development in the MPA in patients with PAH, resulting in an abnormal boundary layer along the wall of the MPA. François et al. (43) and Geiger et al. (44) similarly observed increased vortical flow patterns in the PAs of patients with repaired tetralogy of Fallot. Interestingly, François et al. observed increased PA WSS values in repaired tetralogy of Fallot subjects compared with healthy controls. These studies have demonstrated the feasibility of the technique to elucidate complex 3D flow patterns in the presences of complex anatomy and disease conditions. An important consideration for this technique is that scan times approach 8–15 minutes and the postpreprocessing times vary according to operator experience (≈30 minutes for an experienced user). Although we did not record the processing or scan times, this should be reported in future studies.

Important limitations of this study are that two cohorts were used at each institution and a scan-rescan analysis was not performed. Ideally, the techniques would have been validated using the same subjects at both institutions, with rescans; however, the distance between the institutions precluded the feasibility of conducting a validation study scanning all subjects at both locations. Additionally, the study and its Institutional Review Board–approved protocol were not approved for rescans. Furthermore, given that institution 1 incorporates values measured at both field strengths, intersystem variability is an important consideration. Thus, it is noted that the field dependence of hemodynamic measurements in healthy volunteers were investigated at 1.5T and 3.0T and showed no significant difference for peak velocity, stroke volume, and WSS (45). The spectrum of disease expression and the age difference between the control and PAH population may have added additional heterogeneity to the results. The spatial resolutions used between the two sites were different (2.2–2.75 × 2.2–2.75 × 2.4–3.2 mm, vs. 1.3 mm isotropic); nonetheless, it has been shown previously that bulk flow parameters and WSS are minimally affected in vessels on the size order of the MPA, LPA, and RPA and the chosen range of spatial resolution (26). Despite these limitations, the lack of any significant difference between the parameters measured in healthy subjects or PAH patients and the corroboration with other 2D single-site studies indicates that these techniques can be considered equivalent for flow quantification and WSS calculation (11,19).

In conclusion, CMR using breath-hold CINE balanced steady-state free precession sequences is already considered the gold standard for measuring ventricular size and function (5–10)—particularly of the right ventricle, due to its complex shape, which limits the accuracy of echocardiography. As a result, CMR is increasingly being used to follow and manage patients with PAH. We have demonstrated that 4D flow MRI provides similar bulk flow and WSS values whether using Cartesian or radial acquisitions and that the addition of 4D flow MRI to the standard CMR protocols used to evaluate these patients may permit further characterization of disease severity or monitor changes pulmonary vascular hemodynamics following therapy. Furthermore, the future acquisition of biomechanical properties in the central PAs (such as distensibility) may extend our understanding of PA–RV interactions and how they ultimately impact RV function and failure.

ACKNOWLEDGEMENTS

We thank Alejandro Munoz for support with statistical analysis.

REFERENCES

1. McLaughlin VV, Archer SL, Badesch DB, et al. ACCF/AHA 2009 expert consensus document on pulmonary hypertension: a report of the American College of Cardiology Foundation Task Force on Expert Consensus Documents and the American Heart Association: developed in collaboration with the American College of Chest Physicians, American Thoracic Society, Inc., and the Pulmonary Hypertension Association. Circulation 2009;119:2250–2294.
2. Shah SJ. Pulmonary hypertension. JAMA 2012;308:1366–1374.
3. Thenappan T, Shah SJ, Rich S, Tian L, Archer SL, Gomberg-Maitland M. Survival in pulmonary arterial hypertension: a reappraisal of the NIH risk stratification equation. Eur Respir J 2010;35:1079–1087.
4. Simonneau G, Gatzoulis MA, Adatia I, et al. Updated clinical classification of pulmonary hypertension. J Am Coll Cardiol 2013;62:D34–D41.
5. Clay S, Alfakih K, Messroghli DR, Jones T, Ridgway JP, Sivananthan MU. The reproducibility of left ventricular volume and mass measurements: a comparison between dual-inversion-recovery black-blood sequence and SSFP. Eur Radiol 2006;16:32–37.
6. Hudsmith LE, Petersen SE, Francis JM, Robson MD, Neubauer S. Normal human left and right ventricular and left atrial dimensions using steady state free precession magnetic resonance imaging. J Cardiovasc Magn Reson 2005;7:775–782.

7. Maceira AM, Prasad SK, Khan M, Pennell DJ. Normalized left ventricular systolic and diastolic function by steady state free precession cardiovascular magnetic resonance. J Cardiovasc Magn Reson 2006;8:417–426.
8. Grothues F, Moon JC, Bellenger NG, Smith GS, Klein HU, Pennell DJ. Interstudy reproducibility of right ventricular volumes, function, and mass with cardiovascular magnetic resonance. Am Heart J 2004;147: 218–223.
9. Catalano O, Antonaci S, Opasich C, Moro G, Mussida M, Perotti M, Calsamiglia G, Frascaroli M, Baldi M, Cobelli F. Intra-observer and interobserver reproducibility of right ventricle volumes, function and mass by cardiac magnetic resonance. J Cardiovasc Med (Hagerstown) 2007;8:807–814.
10. Maceira AM, Prasad SK, Khan M, Pennell DJ. Reference right ventricular systolic and diastolic function normalized to age, gender and body surface area from steady-state free precession cardiovascular magnetic resonance. Eur Heart J 2006;27:2879–2888.
11. Ley S, Mereles D, Puderbach M, Gruenig E, Schock H, Eichinger M, Ley-Zaporozhan J, Fink C, Kauczor HU. Value of MR phase-contrast flow measurements for functional assessment of pulmonary arterial hypertension. Eur Radiol 2007;17:1892–1897.
12. Hunter KS, Lee PF, Lanning CJ, Ivy DD, Kirby KS, Claussen LR, Chan KC, Shandas R. Pulmonary vascular input impedance is a combined measure of pulmonary vascular resistance and stiffness and predicts clinical outcomes better than pulmonary vascular resistance alone in pediatric patients with pulmonary hypertension. Am Heart J 2008; 155:166–174.
13. Reiter G, Reiter U, Kovacs G, Kainz B, Schmidt K, Maier R, Olschewski H, Rienmueller R. Magnetic resonance-derived 3-dimensional blood flow patterns in the main pulmonary artery as a marker of pulmonary hypertension and a measure of elevated mean pulmonary arterial pressure. Circ Cardiovasc Imaging 2008;1:23–30.
14. Ooi CY, Wang Z, Tabima DM, Eickhoff JC, Chesler NC. The role of collagen in extralobar pulmonary artery stiffening in response to hypoxia-induced pulmonary hypertension. Am J Physiol Heart Circ Physiol 2010;299:H1823–H1831.
15. Kobs RW, Muvarak NE, Eickhoff JC, Chesler NC. Linked mechanical and biological aspects of remodeling in mouse pulmonary arteries with hypoxia-induced hypertension. Am J Physiol Heart Circ Physiol 2005;288:H1209–H1217.
16. Lammers SR, Kao PH, Qi HJ, Hunter K, Lanning C, Albietz J, Hofmeister S, Mecham R, Stenmark KR, Shandas R. Changes in the structure-function relationship of elastin and its impact on the proximal pulmonary arterial mechanics of hypertensive calves. Am J Physiol Heart C 2008;295:H1451–H1459.
17. Wang Z, Chesler NC. Pulmonary vascular wall stiffness: an important contributor to the increased right ventricular afterload with pulmonary hypertension. Pulm Circ 2011;1:212–223.
18. Reiter U, Reiter G, Kovacs G, Stalder AF, Gulsun MA, Greiser A, Olschewski H, Fuchsjager M. Evaluation of elevated mean pulmonary arterial pressure based on magnetic resonance 4D velocity mapping: comparison of visualization techniques. PloS One 2013;8:e82212.
19. Truong U, Fonseca B, Dunning J, Burgett S, Lanning C, Ivy DD, Shandas R, Hunter K, Barker AJ. Wall shear stress measured by phase contrast cardiovascular magnetic resonance in children and adolescents with pulmonary arterial hypertension. J Cardiovasc Magn Reson 2013;15:81.
20. Tang BT, Pickard SS, Chan FP, Tsao PS, Taylor CA, Feinstein JA. Wall shear stress is decreased in the pulmonary arteries of patients with pulmonary arterial hypertension: an image-based, computational fluid dynamics study. Pulm Circ 2012;2:470–476.
21. Wang Z, Lakes RS, Golob M, Eickhoff JC, Chesler NC. Changes in large pulmonary arterial viscoelasticity in chronic pulmonary hypertension. PloS one 2013;8:e78569.
22. Markl M, Kilner PJ, Ebbers T. Comprehensive 4D velocity mapping of the heart and great vessels by cardiovascular magnetic resonance. J Cardiovasc Magn Reson 2011;13:7.
23. Markl M, Harloff A, Bley TA, Zaitsev M, Jung B, Weigang E, Langer M, Hennig J, Frydrychowicz A. Time-resolved 3D MR velocity mapping at 3T: improved navigator-gated assessment of vascular anatomy and blood flow. J Magn Reson Imaging 2007;25:824–831.
24. Gu T, Korosec FR, Block WF, Fain SB, Turk Q, Lum D, Zhou Y, Grist TM, Haughton V, Mistretta CA. PC VIPR: a high-speed 3D phase-contrast method for flow quantification and high-resolution angiography. AJNR Am J Neuroradiol 2005;26:743–749.
25. Liu J, Wieben O, Jung Y, Samsonov AA, Reeder SB, Block WF. Single breathhold cardiac CINE imaging with multi-echo three-dimensional hybrid radial SSFP acquisition. J Magn Reson Imaging 2010;32:434–440.
26. Stalder AF, Russe MF, Frydrychowicz A, Bock J, Hennig J, Markl M. Quantitative 2D and 3D phase contrast MRI: optimized analysis of blood flow and vessel wall parameters. Magn Reson Med 2008;60:1218–1231.
27. Bock J, Kreher BW, Hennig J, Markl M. Optimized Pre-processing of Time-resolved 2D and 3D Phase Contrast MRI Data. In Proceedings of the 15th Annual Meeting of ISMRM, Berlin, Germany, 2007. p. 3138.
28. Gatehouse PD, Rolf MP, Graves MJ, et al. Flow measurement by cardiovascular magnetic resonance: a multi-centre multi-vendor study of background phase offset errors that can compromise the accuracy of derived regurgitant or shunt flow measurements. J Cardiovasc Magn Reson 2010;12:5.
29. Schiebler ML, Bhalla S, Runo J, Jarjour N, Roldan A, Chesler N, Francois CJ. Magnetic resonance and computed tomography imaging of the structural and functional changes of pulmonary arterial hypertension. J Thorac Imaging 2013;28:178–193.
30. Chien S, Li S, Shyy YJ. Effects of mechanical forces on signal transduction and gene expression in endothelial cells. Hypertension 1998; 31:162–169.
31. Davies PF. Flow-mediated endothelial mechanotransduction. Physiol Rev 1995;75:519–560.
32. Krams R, Cheng C, Helderman F, et al. Shear stress is associated with markers of plaque vulnerability and MMP-9 activity. EuroIntervention 2006;2:250–256.
33. Cheng C, Tempel D, van Haperen R, van der Baan A, Grosveld F, Daemen MJ, Krams R, de Crom R. Atherosclerotic lesion size and vulnerability are determined by patterns of fluid shear stress. Circulation 2006;113:2744–2753.
34. Malek AM, Alper SL, Izumo S. Hemodynamic shear stress and its role in atherosclerosis. JAMA 1999;282:2035–2042.
35. Malek AM, Zhang J, Jiang J, Alper SL, Izumo S. Endothelin-1 gene suppression by shear stress: pharmacological evaluation of the role of tyrosine kinase, intracellular calcium, cytoskeleton, and mechanosensitive channels. J Mol Cell Cardiol 1999;31:387–399.
36. Malek AM, Izumo S, Alper SL. Modulation by pathophysiological stimuli of the shear stress-induced up-regulation of endothelial nitric oxide synthase expression in endothelial cells. Neurosurgery 1999;45: 334–344; discussion 344–335.
37. Malek AM, Jiang L, Lee I, Sessa WC, Izumo S, Alper SL. Induction of nitric oxide synthase mRNA by shear stress requires intracellular calcium and G-protein signals and is modulated by PI 3 kinase. Biochem Biophys Res Commun 1999;254:231–242.
38. Ratnayaka K, Faranesh AZ, Hansen MS, et al. Real-time MRI-guided right heart catheterization in adults using passive catheters. Eur Heart J 2013;34:380–389.
39. Swift AJ, Rajaram S, Hurdman J, et al. Noninvasive estimation of PA pressure, flow, and resistance with CMR imaging: derivation and prospective validation study from the ASPIRE registry. JACC Cardiovasc Imaging 2013;6:1036–1047.
40. Frydrychowicz A, Berger A, Russe MF, Stalder AF, Harloff A, Dittrich S, Hennig J, Langer M, Markl M. Time-resolved magnetic resonance angiography and flow-sensitive 4-dimensional magnetic resonance imaging at 3 Tesla for blood flow and wall shear stress analysis. J Thorac Cardiovasc Surg 2008;136:400–407.
41. Harloff A, Nussbaumer A, Bauer S, Stalder AF, Frydrychowicz A, Weiller C, Hennig J, Markl M. In vivo assessment of wall shear stress in the atherosclerotic aorta using flow-sensitive 4D MRI. Magn Reson Med 2010;63:1529–1536.
42. Bieging ET, Frydrychowicz A, Wentland A, Landgraf BR, Johnson KM, Wieben O, Francois CJ. In vivo three-dimensional MR wall shear stress estimation in ascending aortic dilatation. J Magn Reson Imaging 2011;33:589–597.
43. Francois CJ, Srinivasan S, Schiebler ML, Reeder SB, Niespodzany E, Landgraf BR, Wieben O, Frydrychowicz A. 4D cardiovascular magnetic resonance velocity mapping of alterations of right heart flow patterns and main pulmonary artery hemodynamics in tetralogy of Fallot. J Cardiovasc Magn Reson 2012;14:16.
44. Geiger J, Markl M, Jung B, Grohmann J, Stiller B, Langer M, Arnold R. 4D-MR flow analysis in patients after repair for tetralogy of Fallot. Eur Radiol 2011;21:1651–1657.
45. Strecker C, Harloff A, Wallis W, Markl M. Flow-sensitive 4D MRI of the thoracic aorta: comparison of image quality, quantitative flow, and wall parameters at 1.5 T and 3 T. J Magn Reson Imaging 2012;36: 1097–1103.